

A Study of Standing-Wave Thermoacoustic Refrigerator

Patcharin Saechan, Isaacs Dhuchakallaya

Abstract—Thermoacoustic refrigerator is a cooling device which uses the acoustic waves to produce the cooling effect. The aim of this paper is to explore the experimental and numerical feasibility of a standing-wave thermoacoustic refrigerator. The effects of the stack length, position of stack and operating frequency on the cooling performance are carried out. The circular pore stacks are tested under the atmospheric pressure. A low-cost loudspeaker is used as an acoustic driver. The results show that the location of stack installed in resonator tube has a greater effect on the cooling performance, than the stack length and operating frequency, respectively. The temperature difference across the ends of stack can be generated up to 13.7°C, and the temperature of cold-end is dropped down by 5.3°C from the ambient temperature.

Keywords—Cooling performance, Refrigerator, Standing-wave, Thermoacoustics.

I. INTRODUCTION

DUE to environmental concern caused by the current vapour-compression refrigeration system applying the environmentally hazardous refrigerants such as R134a, R12, the design and development of refrigerating systems particularly in the domestic refrigeration is becoming increasingly important. In order to restrict on the use of such refrigerants, research efforts have been made to develop the alternative refrigerants and novelty refrigeration technologies [1]-[4]. A thermoacoustic refrigeration is a kind of the novel technologies which is environmentally friendly by using inert gases or simply air as working fluids. These gases do not contain any toxic, flammable or ozone depleting substances comparing with the common refrigerants used in the present commercial refrigerators. In addition, thermoacoustic refrigeration has a simple structure and no moving parts which is beneficial such as high reliability, low-cost of manufacture and maintenance.

Thermoacoustic refrigeration utilises the sound waves to generate the cooling effect. Within the solid boundaries, the working fluid interacts thermally with the surface of the solid plates aligned appropriately to the direction of wave propagation. The periodic compression and expansion of gas parcels in the flow field, combining with the heat transfer between gas parcels and solid surface within solid boundaries,

yield a heat-pumping cycle. The cooling capacity can be adjusted straightforward by altering the level of sound pressure, unlike the compressor in common refrigeration system which works just in on-off mode.

The main component of the thermoacoustic refrigeration is a porous media namely “stack” which is sandwiched by two heat exchangers, and placed properly inside a resonator tube. The design and construction to achieve the robust, economical, efficient thermoacoustic refrigeration system are significantly the technical challenges. As been discussed in [5]-[7], the cooling performance of thermoacoustic refrigeration is relatively sensitive to the choice of design parameters, thus the optimisation would be required in order to achieve a high efficiency.

Since the first Hofler’s thermoacoustic refrigerator [5] was revealed, many prototypes of thermoacoustic refrigerators have been developed to improve the cooling capacity and their efficiency [8]-[10]. These efforts were made in different ways to enhance their performances. Although the simple standing-wave refrigeration has a lower efficiency due to intrinsic irreversibility comparing with the complex travelling-wave refrigeration, it is an initiation for developing the sophisticated devices and seeking the potential improvements. If the drawbacks of this technology have been solved or restrained, the environmentally friendly thermoacoustic refrigeration system will take the place of the common vapour-compression refrigeration in the future.

The objective of this work is to explore the experimental feasibility of a standing-wave thermoacoustic refrigerator driven by a low-cost loudspeaker. The effects of the length of stack, position of stack placed in resonator tube and operating frequency on the cooling performance are investigated. In addition, the numerical simulations aided by computer programme DELTAEC [11] are modelled in order to validate the experimental results. The simulation results also help in identifying the way to improve the component design.

II. PRINCIPLES OF THERMOACOUSTIC REFRIGERATION

Fig. 1 shows the schematic diagram and basic operation principle of a standing-wave thermoacoustic refrigeration. The system consists of the stack, ambient heat exchanger (AHX) and cold heat exchanger (CHX) placed inside the resonator with closed end. Once the sound is fed from loudspeaker to create a standing wave in the resonator tube, the gas parcels in the system start to oscillate forth-and-back. Considering on a single gas parcel located near the stack plate as shown in the magnified view of Fig. 1, firstly the parcel is moved left to higher pressure region by the peak-to-peak displacement


Patcharin Saechan is with the Department of Mechanical & Aerospace Engineering, Faculty of Engineering, King Mongkut’s University of Technology North Bangkok, Bangsue, Bangkok, 10800, Thailand (e-mail: patcharin.s@eng.kmutnb.ac.th).

Isaacs Dhuchakallaya is with the Department of Mechanical Engineering, Faculty of Engineering, Thammasat University (Rangsit campus), Klong-Luang, Pathumthani, 12120, Thailand (corresponding author, phone: +66(0)25643001-9; fax: +66(0)25643023; e-mail: disares@engr.tu.ac.th).

Next step, the gas parcel oscillates back to the right to its original position. The gas parcel experiences an adiabatic expansion because it moves to a lower pressure region. As the pressure of the parcel is reduced, the temperature also decreases. Finally, the temperature of parcel becomes lower than that of the solid, thus the heat is transferred from the solid to the parcel at constant pressure condition, and the cooled gas volume becomes larger due to thermal expansion. This compression and expansion of gas parcel causes a thermodynamic cycle in which the stack acts as sink and source in the terminal points of the movement of each parcel. Consequently, in each cycle of the sound wave, each gas parcel pumps a little amount of heat from the right of the stack to the left, from cold to hot. This manner is called “thermoacoustic effect”

Figure 1 consists of three parts: (a) A schematic diagram of the device. It shows a stack of layers (AHX, CHX) connected to a resonator. A heat sink (T_h) and a cooling load (T_c) are applied to the stack. A loudspeaker is connected to the resonator. The work done is denoted by \dot{W} . (b) A P-V diagram showing the cycle path 1-2-3-4. The work done is denoted by dW and the heat input is denoted by dq . (c) A plot of pressure $|p|$ and volume $|U|$ versus position x . The pressure $|p|$ is shown as a dashed line and the volume $|U|$ as a solid line.

The diagram illustrates the experimental setup for studying the sound field in a tube. A horizontal tube of total length 122 cm is divided into five segments of 20 cm each by ports P1, P2, P3, P4, and P5. A stack of four tubes is connected to P1, with a distance 'x' from the tube end. A cone is connected to P7, and a loudspeaker is connected to P8. The distance from P7 to the loudspeaker is 35 cm, and the distance from the loudspeaker to the cone is 25 cm. A function generator and amplifier are connected to the loudspeaker. A diagram below shows the four tubes labeled T1, T2, T3, and T4.



thermocouples (T1-T4) placed equally along the stack from the hot end to the cold end. All thermocouples installed are type-K 0.2 mm diameter PFA insulated. Six pressure sensors (P1-P6) are placed equally along the resonator tube, and two pressure sensors (P7-P8) are installed at the reducing cone in order to monitor the pressure amplitude distribution along the system. All pressure transducers are piezoelectric sensors, model 113B28 of PCB PIEZOTRONICS. The signals from the pressure transducers are monitored and analysed by the digital oscilloscope capable of measuring up to a sampling rate of 200 MHz and 2 Gsa/s. All signals of pressure and temperature are recorded by the high-speed data acquisition.

IV. NUMERICAL MODEL

According to the linear acoustic theory of Rott [14], all acoustic variables are taken to be harmonic in time with radian frequency, ω , as,

$$p = p_m + \text{Re}[p_1(x)e^{i\omega t}] \quad (2)$$

$$U = \text{Re}[U_1(x)e^{i\omega t}] \quad (3)$$

$$T = T_m + \text{Re}[T_1(x)e^{i\omega t}] \quad (4)$$

$$\rho = \rho_m + \text{Re}[\rho_1(x)e^{i\omega t}] \quad (5)$$

Substituting these acoustic variables into the continuity, momentum and energy equations and reduced to first-order, we obtain the approximate equations as:

$$\frac{\partial p_1}{\partial x} = -\frac{i\omega\rho_m}{A_g} \frac{U_1}{1-f_v} \quad (6)$$

$$\frac{dU_1}{dx} = -\frac{i\omega A_g}{\rho_m a^2} \left[1 + \frac{(\gamma-1)f_k}{1+\varepsilon_s} \right] p_1 + \frac{\beta(f_k - f_v)}{(1-f_v)(1-\sigma)(1+\varepsilon_s)} \frac{dT_m}{dx} U_1 \quad (7)$$

$$\frac{dT_m}{dx} = \frac{\dot{H}_2 - \frac{1}{2} \text{Re} \left[p_1 \tilde{U}_1 \left(1 - \frac{T_m \beta(f_k - \tilde{f}_v)}{(1+\varepsilon_s)(1+\sigma)(1-f_v)} \right) \right]}{\frac{\rho_m c_p |U_1|^2}{2A_g \omega (1-\sigma) |1-f_v|^2} \text{Im} \left(\tilde{f}_v + \frac{(f_k - \tilde{f}_v)(1+\varepsilon_s f_v / f_k)}{(1+\varepsilon_s)(1+\sigma)} \right) - A_g k - A_s k_s} \quad (8)$$

$$\frac{\partial E_2}{\partial x} = \frac{1}{2} \text{Re} \left[\tilde{U}_1 \frac{\partial p_1}{\partial x} + \tilde{p}_1 \frac{\partial U_1}{\partial x} \right] \quad (9)$$

where

$$f_k = \frac{2J_1[(i-1)r_0/\delta_k]}{J_0[(i-1)r_0/\delta_k](i-1)r_0/\delta_k} \quad (10)$$

$$f_v = \frac{2J_1[(i-1)r_0/\delta_v]}{J_0[(i-1)r_0/\delta_v](i-1)r_0/\delta_v} \quad (11)$$

$$\varepsilon_s = \left(\frac{k\rho_m c_p}{k_s \rho_s c_s} \right)^{1/2} \frac{f_k(1+i)r_0/2\delta_k}{\tanh[(1+i)l/\delta_s]} \quad (12)$$

In order to solve these equations, a computer programme

DELTAEC [11] is aided. The system is simulated as the sequence of segments, such as duct, stack, transducer, etc., given by the user. Due to p_1 and U_1 being complex, this set of 3 coupled equations, (6)-(8), is split into 5 coupled equations for solving 5 variables, $\text{Re}[p_1]$, $\text{Im}[p_1]$, $\text{Re}[U_1]$, $\text{Im}[U_1]$, and T_m . Therefore, in order to integrate the system of these equations, five boundary conditions are required at one end of the segment. These boundary conditions are the mean temperature, and the real and imaginary part of the complex pressure and complex velocity.

Once the boundary conditions are set at the starting end of the segment, the system equations can be solved and the complex amplitudes and temperature found at the other end of the segment. These values become the boundary conditions that are used to solve the appropriate equations for the next segment and so on. Fourth-order Runge-Kutta integration method is employed in this code. The matching of the pressure and volumetric velocity between regions is straightforward. However, obtaining the correct boundary conditions at the end of the resonator, along with the temperature and heat transfer rate at the free end of the segment, is not as easily achieved. In order to meet these boundary conditions requires iteratively adjusting selected upstream variables. This can be achieved by using a shooting method.

V. RESULTS AND DISCUSSION

A. Resonant Frequency

Loudspeaker has a resonant frequency similar to all suspending objects. At this frequency, it will vibrate most freely. This can imply that its voice coil will vibrate with the maximum amplitude and velocity. Thus, the resonant frequency should be the operating frequency of the system. A simple and reliable method to determine the resonant frequency is described by [15]. By adjusting the frequency in the range of the specified resonance, the point that a maximum voltage across the loudspeaker is observed is defined as the resonant frequency. In addition, the resonant frequency of system can also be determined by measuring the pressure amplitude of gas in the resonator tube as function of the frequency. When a peak of pressure amplitude is detected, the resonance takes place.

In Fig. 4, as the signal frequency is adjusted, there are two impedance peaks detected at 72 and 160 Hz, respectively. The second peak of impedance is much higher than the first one. Therefore, the operating frequency should be at 160 Hz as considering in terms of impedance. However, at the frequency of 160 Hz, the pressure amplitude of working fluid measured at P1 is very low comparing with at 72 Hz. This inconsistency of impedance and pressure amplitude leads to further investigation.

Pressure sensors (P1-P8) are then installed to measure the pressure distribution along the resonator tube at both resonant frequencies. As shown in Fig. 5, the pressure variation of 72 Hz characterises a quarter-wavelength manner, while one wavelength form can be comparative to the pressure distribution for case of 160 Hz. As been reported by Swift

[13], the thermoacoustic effect is strengthened with pressure amplitude. Furthermore, the location of stack installed in resonator tube is in between 0-30 cm from the closed end. From this aspect, the frequency of 72 Hz is chosen as the operating condition throughout this work to attain higher cooling performance.

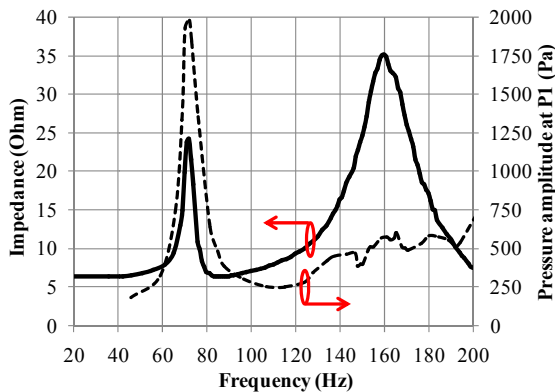


Fig. 4 Loudspeaker impedance and pressure curves

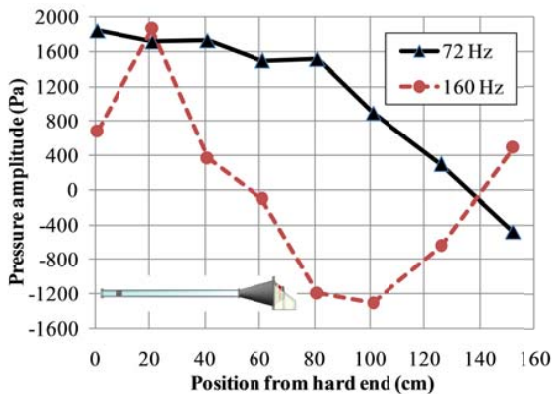


Fig. 5 The distribution of pressure amplitude along the resonator tube

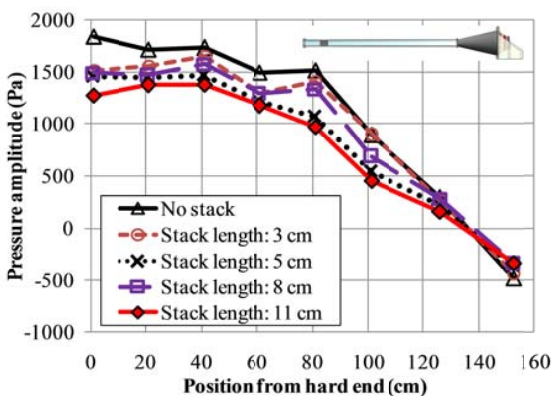


Fig. 6 The change of pressure amplitude as the stack installed at frequency of 72 Hz

Fig. 6 shows the effect of the installed stack on the pressure amplitude in the system. When stack is placed at distance of 10 cm from the closed end to the centre of stack, all pressure

amplitudes in resonator tube reduce due to viscous loss caused by stack; and the pressure amplitudes continue decrease as the length of stack becomes longer. It is notable that all profiles of pressure variation also resemble to a quarter-wavelength.

B. Cooling Performance Tests

In each experiment, all data reading from thermocouples and pressure sensors are recorded since the loudspeaker is actuated until the system becomes stable. The response of system to the operating frequency, stack length, and position of stack are studied. The cooling performance of system can be represented by the temperature difference across the stack.

The variation of gas temperature within the stack at frequency of 72 Hz, stack length of 8 cm and stack position of 10 cm is shown in Fig. 7. It can be seen that the temperature of hot end (T1) increases suddenly at the beginning and gradually stabilise with time, while the cold end temperature (T4) decrease sharply and becomes stable faster than the opposite side. Other temperatures in the stack, T2 and T3, also illustrate the equally-likely temperature distribution within stack. This temperature measurement is also confirmed by the thermal image as shown in Fig. 8, where the white box is the boundary of stack. The maximum and minimum temperatures captured in the thermal image are around 34.6 and 22.2°C, respectively.

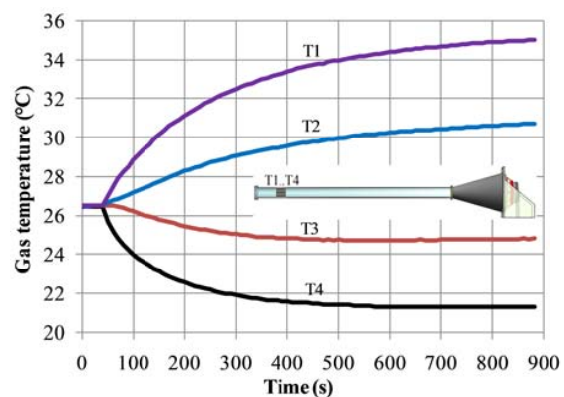


Fig. 7 The history of temperature distribution along the stack

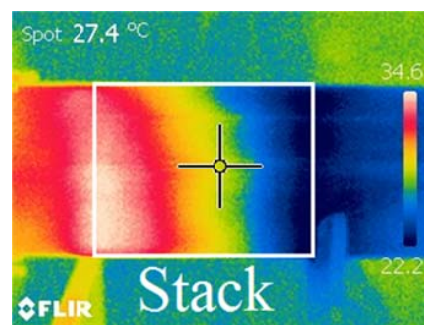


Fig. 8 The thermal image of stack at the same conditions as Fig. 7

C. Comparison of the Numerical and Experimental Results

In order to find out the optimal conditions of the proposed system, the DELTAEC code is constructed to diminish the number of experiments. At the same condition as Fig. 7:

frequency of 72 Hz, stack length of 8 cm and stack position of 10 cm, the pressure amplitude and velocity amplitude distributions shown in Fig. 9 exhibit a quarter-wavelength behaviour, where the maximum velocity is located near the exit of reducing cone, and the maximum pressure is found near the closed end of resonator tube. Thus, the stack should be located near the antinode of pressure in order to accomplish the thermoacoustic effect. As seen, the numerical results can capture well the trend of the measured pressure amplitude. Unfortunately, the velocity of working fluid cannot measure, so the comparison of velocity is not shown here.

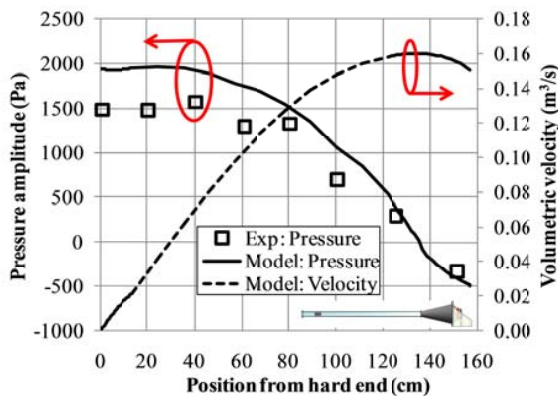


Fig. 9 The pressure amplitude and volumetric velocity amplitude distribution at the same conditions as shown in Fig. 7

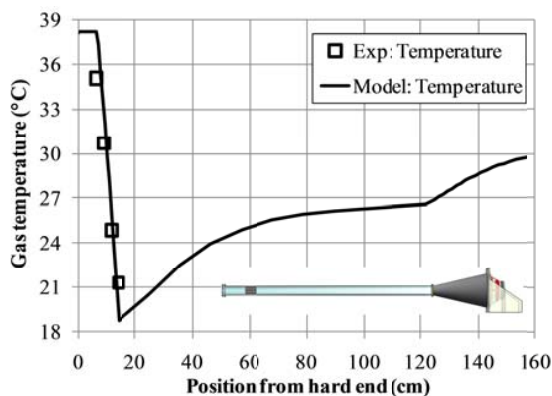


Fig. 10 The gas temperature distribution at the same conditions as shown in Fig. 7

Fig. 10 shows the temperature distribution along the system. The predicted gas temperature decreases continuously from loudspeaker towards stack. This reduction of temperature in resonator tube is caused by heat transfer from surrounding. Within the stack, the temperature increases keenly due to the thermoacoustic effect. As seen, the minimum temperature of 18.7°C at the cold end of stack can be achieved. The temperature measured within stack is in fairly good agreement with the prediction results, except at the both ends of stack. In the experimental results, the temperature difference of 13.7°C and the temperature can be dropped down by 5.3°C from the ambient temperature.

Fig. 11 shows the effect of the operating frequency on the temperature difference across the stack at steady state condition. The centre of each stack is located 10 cm away from closed end. In all stack lengths, the frequency in range of 72-75 Hz can create a peak of maximum temperature difference across the stack, in which this range of frequency corresponds to the resonant frequency of system. For each frequency, the stack length of 8 cm can generate the highest temperature difference, and the stack length of 5 cm performs better than the stack length of 11 cm. Theoretically, the thermoacoustic effect is directly proportional to the stack length. However, as the stack is too long, there will be a significant production of the dissipation, which also reduces the thermoacoustic effect.

The prediction results of DELTAEC also correspond to the experimental results that the frequency in range of 72-75 Hz is appropriate to operate this system. Nevertheless, the magnitudes of temperature difference predicted by DELTAEC are still far from the measurements. It is also noteworthy that the variation of the operating frequency has a less effect on the temperature difference across the stack comparing with the variation of the stack length. Furthermore, the effect of the position of the stack in resonator tube on the cooling performance of the system is carried out. As shown in (7) and (8), the acoustic power is a product of pressure and velocity, and the temperature gradient of stack depends directly on the acoustic power consumed in the stack. As the stack is moved away from the closed end, the pressure amplitude decreases continuously until reaching zero and velocity increases to its peak as shown in Fig. 9. Since the viscous loss is proportional to the square of the velocity, the maximum acoustic power gradient should occur at a position between the pressure antinode and pressure node. Fig. 12 presents the relationship between the maximum temperature difference across stack and the operating frequencies at different stack lengths. As seen, the gradient of temperature increase progressively when the stack is moved towards the closed end, and reaching a peak before dropping suddenly to zero. The DELTAEC results show that as the stack length increases, the location of maximum temperature difference shifts towards the loudspeaker. The optimal location of stack should be in range of 7-10 cm as predicted by simulation. For all experiments, the appropriate position for installing stack is 10 cm away from the closed end to the centre of stack. Again, the DELTAEC can predict reasonably the trends of experimental results, but the magnitude of temperature difference cannot match well.

VI. CONCLUSIONS

A standing-wave thermoacoustic refrigerator driven by a low-cost loudspeaker is designed, constructed, and tested to explore the feasibility of this device. The effects of the stack length, position of stack and operating frequency on the cooling performance are experimentally and numerically studied. Results from the study can conclude that the location of stack installed in resonator tube has a great effect on the cooling performance, and the operating frequency has a less effect on the cooling performance among the parameters

investigated. The measurements also confirm that the performance of this refrigerator is satisfied as expected. A maximum temperature difference up to 13.7°C is achieved, and the temperature can be dropped down by 5.3°C from the ambient temperature.

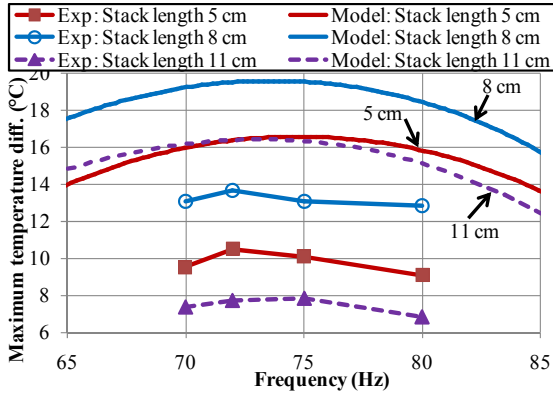


Fig. 11 The relationship of the maximum temperature difference across stack and the operating frequencies at different stack lengths comparing with the DELTAEC predictions

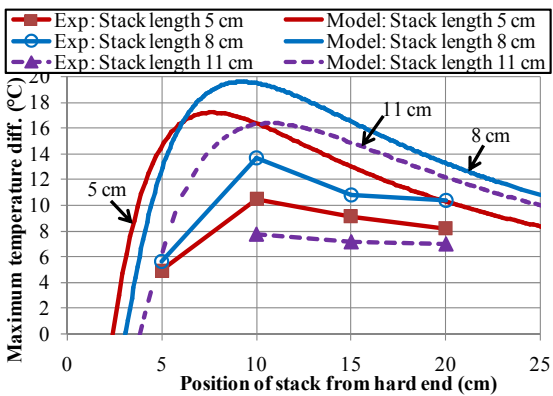


Fig. 12 The relationship of the maximum temperature difference across stack and the positions of stack at various stack lengths comparing with the DELTAEC predictions

NOMENCLATURE

a	Speed of sound, m/s
c_p	Specific heat capacity, J/kg·K
E_2	Acoustic power, W
f	Frequency, Hz
\dot{H}_2	Total power flux, W
h	Thermoviscous function
i	$\sqrt{-1}$
k	Thermal conductivity, W/m·K
p_1	Pressure, Pa
r	Radius, m
r_h	Hydraulic radius, m
T	Temperature, K, °C
t	Time, s
U_1	Volumetric flow rate, m ³ /s
β	Thermal expansion coefficient, K ⁻¹
γ	Ratio of isobaric to isochoric specific heats

Δ	Difference
δ	Penetration depth, m
ε	Internal energy per unit mass, J/kg
ε_s	Correction factor for finite solid heat capacity
κ	Thermal diffusivity, m ² /s
λ	Wavelength, m
μ	Dynamic viscosity, kg/m·s
ν	Kinematic viscosity, m ² /s
ξ	Displacement of gas, m
ρ	Density, kg/m ³
σ	Prandtl number
ω	Angular frequency, s ⁻¹

REFERENCES

- [1] B. Palm, "Hydrocarbons as refrigerants in small heat pump and refrigeration systems – A review," *Int. J. of Refrigeration*, vol. 31, pp. 552-563, 2008.
- [2] I. Sarbu, "A review on substitution strategy of non-ecological refrigerants from vapour compression-based refrigeration, air-conditioning and heat pump systems," *Int. J. of Refrigeration*, vol. 46, pp. 123-141, 2014.
- [3] J. Sarkar, "Ejector enhanced vapor compression refrigeration and heat pump systems—A review," *Renewable and Sustainable Energy Reviews*, vol. 16, pp. 6647-6659, 2012.
- [4] S.L. Garrett, T.J. Hofler, and D.K. Perkins, "Thermoacoustic refrigeration," in *Alternative Fluorocarbons Environmental Acceptability Study, Refrigeration and Air conditioning Technology Workshop*, Breckenridge Hilton, Breckenridge, 1993.
- [5] T.J. Hofler, "Thermoacoustic refrigerator design and performance," in Ph.D Thesis, Physics Department, University of California, San Diego, 1986.
- [6] I. Paek, J.E. Braun, and L. Mongeau, "Evaluation of standing-wave thermoacoustic cycles for cooling applications," *Int. J. of Refrigeration*, vol. 30, pp. 1059-1071, 2007.
- [7] A. Piccolo, "Optimization of thermoacoustic refrigerators using second law analysis," *Applied Energy*, vol. 103, pp. 358-367, 2013.
- [8] S.L. Garrett, J.A. Adeff, and T.J. Hofler, "Thermoacoustic refrigerator for space applications," *J. of Thermophysics and Heat Treansfer*, vol. 7, 1993.
- [9] M.M. Bassem, Y. Ueda, and A. Akisawa, "Design and construction of a traveling wave thermoacoustic refrigerator," *Int. J. of Refrigeration*, vol. 34, pp. 1125-1131, 2011.
- [10] P. Saechan, H. Kang, X. Mao, and A.J. Jaworski, "Thermoacoustic refrigerator driven by a combustion-powered thermoacoustic engine – demonstrator of device for rural areas of developing countries," in *Proceedings of the World Congress on Engineering 2013*, vol. III, London, U.K., 2013.
- [11] B. Ward, J. Clark, and G.W. Swift, "Design Environment for Low-Amplitude ThermoAcoustic Energy Conversion (DELTAEC) programme," version 6.2 b3, Los Alamos National Laboratory, New Mexico, USA, 2008.
- [12] G.W. Swift, "Thermoacoustics," in *Springer Handbook of Acoustics*, T.D. Rossing Ed. Springer, 2007.
- [13] G.W. Swift, "Thermoacoustic engines," *J. of the Acoustical Society of America*, vol. 84, pp. 1145-1180, 1988.
- [14] N. Rott, "Thermoacoustics," *Advances in Applied Mechanics*, vol. 20, pp. 135-175, 1980.
- [15] R. Elliott, "Measuring Loudspeaker Parameters," Available from: <http://sound.westhost.com/tsp.htm> (Accessed 19 January 2015).